Vol. 38, No. 2 (2016) 163-175

Tribology in Industry

www.tribology.fink.rs

RESEARCH

Enhancement of a Constitutive Friction Law by Considering Plastic Smoothing of Rough Surfaces in Dependency on the Bulk Stresses

F. Beyer[a], M. Löffler[b], K. Willner[a], U. Engel[b], M. Merklein[b]

[a] *Chair of Applied Mechanics, Friedrich-Alexander-Universität Erlangen-Nürnberg, Egerlandstr. 5, 91058 Erlangen, Germany,*
[b] *Institute of Manufacturing Technology, Friedrich-Alexander-Universität Erlangen-Nürnberg, Egerlandstr. 11-13, 91058 Erlangen, Germany.*

Keywords:

Friction
Constitutive friction law
Half-space model
Elasto-plastic contact
Strain hardening
Bulk stresses
Sheet-bulk metal forming

Corresponding author:

F. Beyer
Chair of Applied Mechanics,
Friedrich-Alexander-Universität Erlangen-Nürnberg, Egerlandstr. 5, 91058 Erlangen
E-mail: florian.beyer@ltm.uni-erlangen.de

A B S T R A C T

The aim of this work is the improvement of a constitutive friction law which has been identified for the specific demands of sheet-bulk metal-forming. The constitutive friction law determines the friction shear stress in dependency on the plastic smoothing of the surface roughness, which also affects the real contact area. An experimental setup is introduced to determine the change of the surface roughness, which is influenced by the tensile bulk stress in the workpiece. In order to model the experimental results, a well-established half-space model is presented and improved to consider strain hardening. The half-space model is used to determine the change of the contact area as a function of the tensile bulk stress. This interdependency is also reflected by the proposed constitutive friction law.

1. INTRODUCTION

Friction between the die and the workpiece plays a vital role in forming processes. It impacts wear and lifetime of the tool, the flow of the deformed material and the required process forces. Friction is influenced by many factors, for example temperature, sliding velocity, flow stress, and the surface roughness. Although friction has been widely studied, the big amount of factors influencing friction still inhibits a general mathematical formulation of the friction interaction. This is also reflected in the broad range of different friction laws, which are available for the simulation of forming processes. Forming processes are commonly classified into sheet metal processes and bulk forming processes. The Coulomb friction model is an accepted model for the simulation of sheet metal forming, which mostly occurs with low to moderate contact loads. The Coulomb friction model describes the friction shear stress as a function of the normal stress and the friction coefficient. Furthermore, Westeneng proposed a model in [1] that focuses on the boundary lubrication and ploughing regime in order to provide an advanced model especially for

deep drawing. In a similar way, Hol developed a boundary lubrication friction model that relies on the surface deformation of the contacting surfaces [2]. The latter model is designed for the particular needs of automotive sheet metal forming.

On the other hand, bulk forming processes, which take place with very high contact loads, are commonly simulated with the friction model of Tresca. This model estimates the friction stress by using the shear strength of the weaker material in contact and the friction factor. Alternatively, a plastic wave friction model with the ability to take into account mixed lubrication was presented by Vidal-Sallé et al. in [3].

However, forming processes which show characteristics of both sheet metal forming and bulk metal forming make the choice of an applicable friction law difficult. A prime example for this is sheet-bulk metal forming, as bulk forming processes are applied onto metal sheets [4]. The products of sheet-bulk metal forming are lightweight high-precision components with functional integration, which grant this process an outstanding role. Sheet-bulk metal forming comes with both low and high contact loads. Therefore, the friction models of Shaw [[5], [6]], or Wanheim and Bay [[7], [8]] are more suitable, since these laws provide a smooth transition between Coulomb's friction model and Tresca's one. This characteristic is also important for the constitutive friction law (CFL) which is presented in [9].

The CFL is mathematically formulated as:

$$\tau = m \cdot k \cdot \alpha, \tag{1}$$

where τ is the friction shear stress, k is the shear yield strength, and α denotes the contact ratio between the real contact area A_r and the apparent area A_0. The friction factor m has to be measured experimentally, for instance by ring upsetting [10]. Due to the roughness of technical surfaces, A_0 is only in contact with its surface asperities. The area which is provided by these asperities is A_r. The parameter α is a relevant indicator as contact loads are only transferable in A_r, or by hydrodynamic effects.

The CFL distinguishes between initial contact and un-/reloading. For initial contact α is identified similar to the findings of Shaw as:

$$\alpha = \sqrt[a_1]{\tanh\left(b_1 \cdot \frac{p_{mean}}{H}\right)^{a_1}}, \tag{2}$$

where p_{mean} is the contact pressure acting on A_0, H is the surface hardness and a_1 and b_1 are numerically identified parameters.

As the CFL is the product of the shear strength and the contact ratio, it can be interpreted as Tresca's friction law taking effect only in A_r. Due to the plastic deformation of the surface, A_r increases linearly with p_{mean} for low to moderate contact loads. Since A_r cannot surpass A_0, α approaches 100% for large p_{mean}. For low contact loads the CFL shows a behavior similar to Coulomb's friction law. Yet, for high contact loads, the CFL is related to Tresca's law of friction. A qualitative comparison between Tresca's law, Coulomb's law and the CFL is shown in Fig. 1.

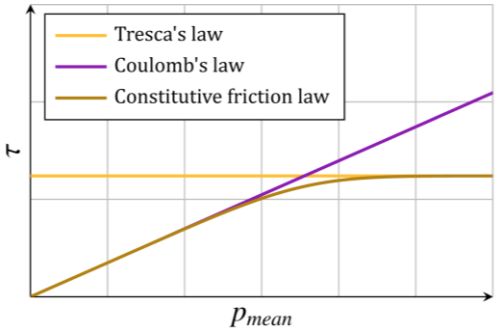

Fig. 1. Qualitative comparison of friction models.

As sheet-bulk metal forming can occur incrementally, the CFL is able to take into account un- and reloading. Un-/reloading is mostly elastic, since the plastic surface deformation already occurred at the initial contact. For un-/reloading the CFL is also expressed by Eq. (1), but with an altered α:

$$\alpha = \sqrt[a_2]{\tanh\left(\frac{b_2}{\alpha(p_h)} \cdot \frac{p_{mean}}{H}\right)^{a_2}} \cdot \alpha(p_h). \tag{3}$$

In Eq. (3) the parameters a_2 and b_2 are identified numerically. Additionally, α for un-/reloading depends on the historic contact load p_h, which is the maximum contact load of the previous contacts. The parameter $\alpha(p_h)$ takes into account the plastic surface smoothing which arose in a previous contact step with p_h. This leads to a real contact area for un-/reloading which is larger than the real contact area at initial contact. Fig. 2

shows the progression of τ for initial contact and for un-/reloading.

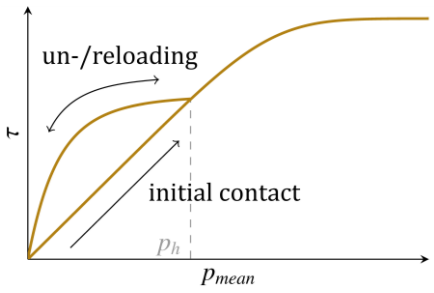

Fig. 2. Friction law with un- and reloading.

Certainly, sheet-bulk metal forming is also characterized by local highly varying two-dimensional and three-dimensional stress and strain states in the bulk material. This condition is not incorporated by the CFL.

In order to identify α in dependency on the bulk stress, the elastic-plastic half-space model which was used in [9] has to be enhanced. Sec. 2 describes this half-space model and provides, additionally, an implementation that considers the surface smoothing as a function of the strain hardening and bulk stresses. That followed, an experimental set-up is described in Sec. 3, which enables the determination of the surface smoothing in dependency on the tensile stress in the bulk material. Sec. 4 describes the subsequent validation and calibration of the half-space model using the experimental results. In Sec. 4 the newly developed CFL is described.

2. NUMERICAL MODEL

2.1 Elastic Half-Space Model

The contact between rough surfaces is a multi-scale problem. Hence, the investigated surfaces have to be large enough to be representative. Moreover, the surface discretization has to be very fine. The finite element method is a viable method for such a challenge due to its universality, as shown in [[11], [12], [13]].

However, a half-space model is preferred because such a model only needs to solve the contact problem at the two-dimensional surface boundary [14]. Hereafter, the complexity of the half-space model is much lower than the one of the finite element method.

The elastic half-space model is based on the work of Tian and Bhushan [15], which is a well-established method for the contact simulation between two linear elastic bodies. The surface of each body is discretized into $N_x \times N_y = M$ elements on a regular grid with element size $2a \times 2b$. Fig. 3 illustrates an example with $N_x \times N_y = 4 \times 3$ elements for the length L_x in x-direction and L_y in y-direction.

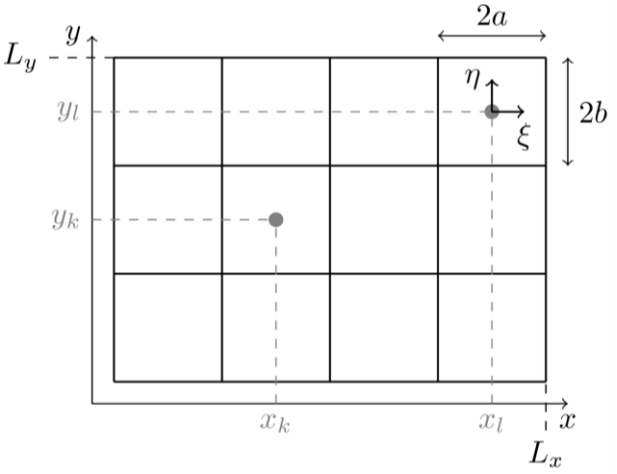

Fig. 3. Top view of discretized surface.

The surface deformation is defined by the following three equations:

$$g_k = h_{max} - h_k + u_k - u_0, \tag{4}$$

$$\sum_{k=1}^{M} p_k \cdot 2a \cdot 2b = p_{mean} \cdot L_x \cdot L_y, \tag{5}$$

$$u_k = \sum_{l=1}^{M} C_{kl} \cdot p_l. \tag{6}$$

Eq. (4) determines the gap g_k of the surface element k in dependency on the maximum height h_{max} of the rough surface, the local height h_k of element k, the local surface deformation u_k and the global body approach u_0. The interrelationship between the variables is shown in Fig. 4.

The condition of equilibrium is defined by Eq. (5). The latter shows that the mean contact pressure p_{mean} acting on the whole discretized area $L_x \times L_y$ has to be in balance with the sum of the local contact pressure p_k. The contact pressure p_k is nonzero only for the elements l that are in actual contact.

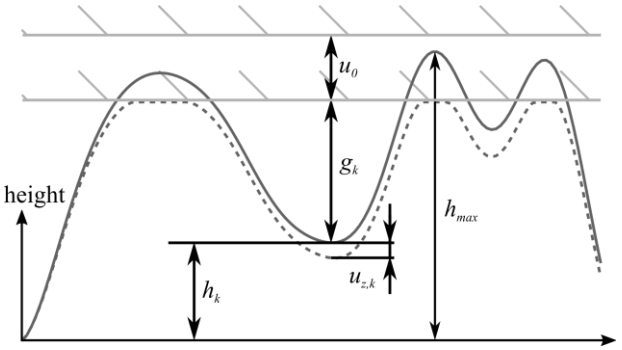

Fig. 4. Definition of notation for gap equation.

The surface deformation at k due to the load at element l is described by Eq. (6), which is based on the analytic Boussinesq solution [16]. The influence coefficient matrix C_{kl} is:

$$C_{kl} = \frac{1}{\pi E^*} \int_{-a}^{a} \int_{-b}^{b} \frac{d\xi d\eta}{\rho}, \tag{7}$$

where the effective elastic modulus E^* is defined as:

$$\frac{1}{E^*} = \frac{1-\nu_1^2}{E_1} + \frac{1-\nu^2}{E_2}, \tag{8}$$

with E_i and ν_i as Young's moduli and Poisson's ratios of the contacting bodies, respectively. In addition, the distance between the load point l and the field point k is given by:

$$\rho = \sqrt{(x_k - x_l - \xi)^2 + (y_k - y_l - \eta)^2}. \tag{9}$$

Love presented in [17] a solution to Eq. (7):

$$\begin{aligned} C_{kl} = \frac{1}{\pi E^*} \Bigg[& x_1 \ln\left(\frac{y_1 + \sqrt{x_1^2 + y_1^2}}{y_2 + \sqrt{x_1^2 + y_2^2}}\right) \\ & + x_2 \ln\left(\frac{y_2 + \sqrt{x_2^2 + y_2^2}}{y_1 + \sqrt{x_2^2 + y_1^2}}\right) \\ & + \mathrm{y}_1 \ln\left(\frac{\mathrm{x}_1 + \sqrt{\mathrm{x}_1^2 + \mathrm{y}_1^2}}{\mathrm{x}_2 + \sqrt{\mathrm{x}_2^2 + \mathrm{y}_1^2}}\right) \\ & + y_2 \ln\left(\frac{x_2 + \sqrt{x_2^2 + y_2^2}}{x_1 + \sqrt{x_1^2 + y_2^2}}\right) \Bigg], \end{aligned} \tag{10}$$

with

$$x_1 = x + a, \qquad x_2 = x - a, \tag{11}$$

and

$$y_1 = y + b, \qquad y_2 = y - b. \tag{12}$$

The contact occurs neither with penetration nor with adhesion. Therefore, the system which determines the surface deformation, i.e., Eqs. (4) to (6), has to be solved in conjunction with the complementarity conditions, which are given by the two equations:

$$g_k = 0, \qquad p_k > 0, \qquad k \in I_C \tag{13}$$

and

$$g_k > 0, \qquad p_k = 0, \qquad k \notin I_C, \tag{14}$$

where I_c is a set including all elements that are in contact.

As it is described in detail by Allwood in [18], the nonlinear contact problem for elastic contact is efficiently solved for the target p_{mean} by using an active set strategy in combination with the conjugate gradient method.

2.2 The Elastic-Plastic Half-Space Model With Work Hardening

The elastic contact model is extended to an elastic-plastic contact model by limiting the local contact pressure p_k by the surface hardness of the softer contacting material H, i.e.,

$$p_k \leq H, l = 1, \ldots, M. \tag{15}$$

According to Bowden and Tabor [19], H depends on the yield strength σ_y with:

$$H \approx 2.8 \cdot \sigma_y. \tag{16}$$

In addition, the surface displacement u_k is divided additively into an elastic surface displacement $u_{el,k}$ and a plastic surface displacement $u_{pl,k}$,

$$u_k = u_{el,k} + u_{pl,k}. \tag{17}$$

The determination of the plastic deformation for p_{mean} is performed after the evaluation of the solely elastic solution for the same p_{mean}. As it is described in detail in [20], contact elements with a local contact pressure that surpasses the local hardness H_k are added to a 'plastic set', in which p_k is defined as:

$$p_k = H_k. \tag{18}$$

That followed, the deformation $u_{pl,k}$, due to the elements in the plastic set, as well as its resulting load p_{pl} are determined. The gap equation (4) is reformulated by:

$$g_k = h_{max} - h_k + u_{el,k} + u_{pl,k} - u_0, \tag{19}$$

which has to be solved for an updated p_{mean} subtracted by p_{pl}. The plastic surface

displacement has to be determined iteratively, until the elastic solution and Eqs. (17) to (19) are converged.

The hitherto described model considers ideal elastic-plastic material behavior with a constant hardness. The next extension of the contact model aims to model the plasticity with the Hockett-Sherby hardening law [21]. This non-linear hardening function describes σ_y in dependency on the true strain ε as:

$$\sigma_y = \sigma_\infty + (\sigma_0 - \sigma_\infty) \cdot \exp\left(a_{HS} \cdot \varepsilon^{b_{HS}}\right), \quad (20)$$

where the initial and infinite yield strength are denoted by σ_0 and σ_∞, respectively, and the curvature multipliers are denoted by a_{HS} and b_{HS}. The reference height λ is necessary to determine ε of a surface element, since the actual length of an element in a half-space model is infinite. Inspired by Hol [2] the true strain ε_k of element k is defined as:

$$\varepsilon_k = \ln\left(1 + \frac{u_{pl,k}}{\lambda}\right), \quad (21)$$

where the characteristic length λ is assumed to be equal for each surface element.

Further, the contact model also considers volume conservation based on the experimental results of Pullen and Williamson [22]. As shown in Fig. 5, the volume which is displaced due to the plastic deformation of the surface asperities is evenly added to the surface valleys which are not in contact.

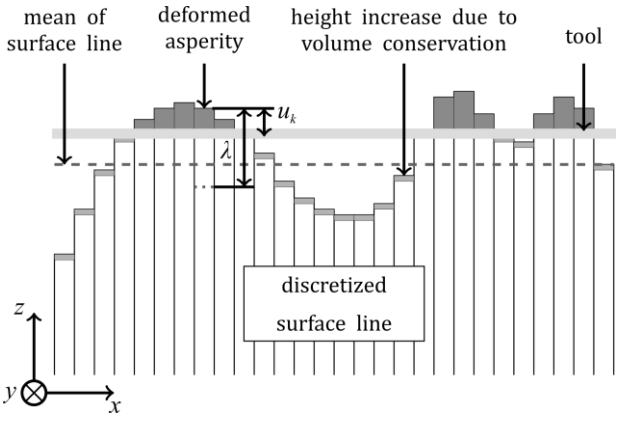

Fig. 5. Definition of λ and example for volume conservation.

This contact model solves the contact problem in dependency on the interfacial pressure. However, it does not take into account the stress and strain condition in the bulk. Three-dimensional contact models which are based on the Boussinesq solution and take into account such stress and strain rates have been proposed for example by Jacq et al. [23] for rolling contact, and by Nélias et al. [24] in combination with a von Mises yield criterion. According to Johnson [25], there exist three different contact zones, this being the elastic zone, the elastic-plastic zone, and the full plastic zone. Contact models such as the ones presented in [[23], [24]] are especially suited for the elastic-plastic regime [26].

As the contact loads are very large in the following experimental setup, the focus of this study is the fully plastic regime. This allows to apply the presented contact model and brings the advantage of reduced numerical effort. The disadvantage of the simplified contact model is the inability to directly take into account bulk stresses. Therefore, the surface hardness is also expressed in dependency on the bulk stress:

$$\left(\frac{p_k}{\beta}\right)^2 + \left(\frac{\sigma_x}{\gamma}\right)^2 + \frac{p_k \cdot \sigma_x}{\beta \cdot \gamma} \leq \sigma_{y,k}^2. \quad (22)$$

The latter is a relation motivated by the Tabor equation [27]. The tensile stress is denoted by σ_x and the parameters β and γ are factors which are identified in Sec. 4.2.

3. EXPERIMENTAL SETUP

A test rig was developed to determine the roughness smoothing in dependency on p_{mean} and the bulk stress σ_x. It is shown in Fig. 6.

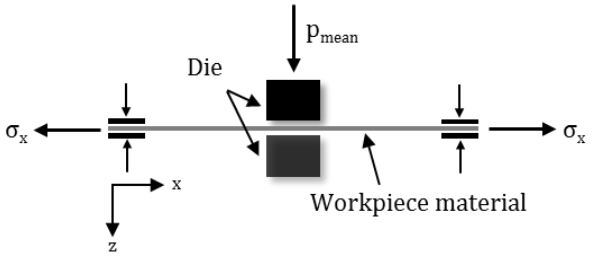

Fig. 6. Experimental setup.

The workpiece material, with the dimensions 300 mm x 30 mm and an initial thickness of 2 mm, is clamped on both sides. The bulk stress σ_x is applied on the workpiece material in x-direction. The values of σ_x are proportional to σ_0 of the investigated material and varied from 0 to $1.0 \cdot \sigma_0$ in steps of $0.25 \cdot \sigma_0$. These values guarantee a broad investigation of the pre-strain on the

surface smoothing. The bulk stress is superimposed by p_{mean}, which is applied due to the movement of the upper punch in z-direction. The chosen values for p_{mean} depend on the material. The experiments were conducted using DC04 and DP600 with electrical discharge texturing (EDT) surfaces. For DC04, p_{mean} took the values 100, 250, 500 and 750 N/mm^2. As the yield strength of DP600 is more than twice as high as that of DC04, the value 1000 N/mm^2 was also included in the experiment with DP600. The analyses are realized without using a lubricant between punch and workpiece. By doing this, the influence of lubrication, like viscosity, is avoided. To ensure a dry contact condition, the workpiece surface was cleaned with acetone. The surface texture before and after the experiments were measured using the confocal laser scanning microscope Keyence VK-X200. An area of 2.63 mm x 2.81 mm was measured to guarantee stable roughness values. The measurements were performed with an objective lens with an optical magnification of 20x.

4. RESULTS

4.1 Experimental Results

In order to validate the numerical results, the surface smoothing as a function of the nominal contact load and the bulk stress was determined experimentally. Exemplary topographies are illustrated, to investigate the smoothing qualitatively. The surface smoothing is quantified by means of R_{a_ref}. This value is the R_a value after forming referenced to the initial average roughness value of the DC04 blanks which amounts to 0.94 ± 0.01 µm. Thus, the smoothening is investigated using the change of the average roughness value.

Fig. *7* shows the impact of using different p_{mean} on the topography of a DC04 blank without applying an additional bulk stress. An increase of the nominal contact load from 250 N/mm^2 to 750 N/mm^2 leads to a significant smoothing of the surface. The higher the load the higher the flattening is. This qualitative correlation can be verified by comparing the referenced average roughness values, see Fig. 8. A high value of p_{mean} results in higher smoothing of the surface. A significant decrease of R_{a_ref} can be observed for the load values 250 N/mm^2, 500 and 750 N/mm^2. Yet, a contact load of 100 N/mm^2 leads to only a slight flattening of the surface. The nominal contact load of 100 N/mm^2 is not high enough to significantly plastically deform the material. All in all, it can be stated that the application of just a nominal contact load and thus a uniaxial stress state leads to a significant height reduction of the roughness peaks and, thus, to an increased smoothing of the surface. Additionally, the dimension of the height reduction is highly influenced by the amount of the applied load.

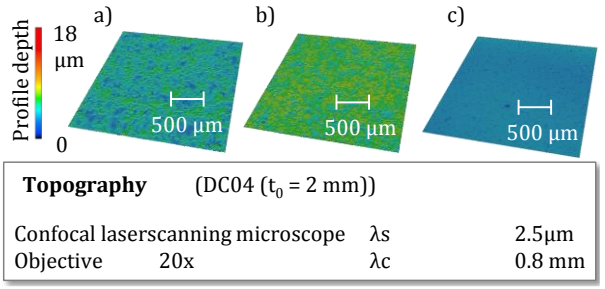

Fig. 7. Topographies of a) an initial DC04 blank, b) the surface after applying a nominal contact load of b) 250 N/mm^2 and c) 750 N/mm^2

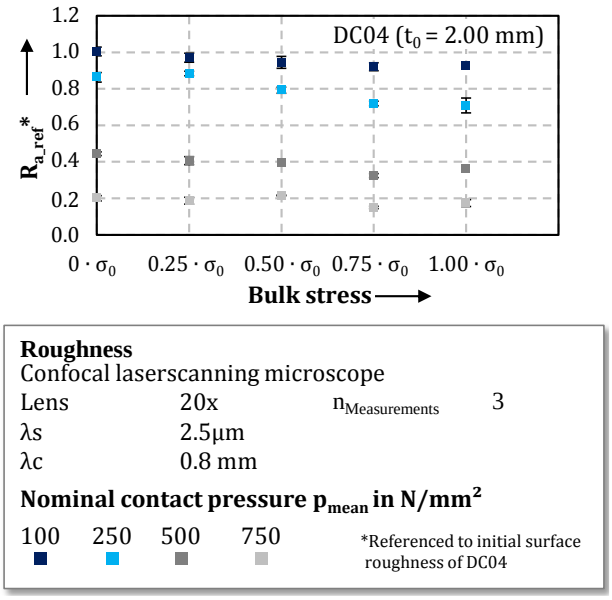

Fig. 8. Average roughness values in dependence on bulk stress and nominal contact load referenced to initial surface roughness for DC04.

The combined application of a nominal contact load and a bulk stress additionally influences the surface smoothing. Thus, the flattening of the surface is strengthened due to the application of an additional bulk stress. However, the influence of the applied bulk stress is not as distinctive as the one of the nominal contact load.

An increase of the applied bulk stress leads to a slight decrease of the R_{a_ref} values. For a nominal contact load of 500 N/mm² the R_{a_ref}. value constantly decreases from 0.44 ± 0.01 µm for $0{\cdot}\sigma_0$ to 0.36 ± 0.01 µm for $1{\cdot}\sigma_0$. Thus, the flattening of the roughness peaks increases with increasing bulk stress values due to the two-dimensional stress state. The same tendencies are valid for the other investigated nominal contact loads.

Additionally, Fig. 9 shows the topographies of DC04 blanks for a nominal contact load of 250 N/mm² with varying bulk stresses. The topographies verify the results of the quantitative investigation using R_{a_ref}. It can be observed that an increase of the bulk stress leads to a more flat profile of the roughness peaks.

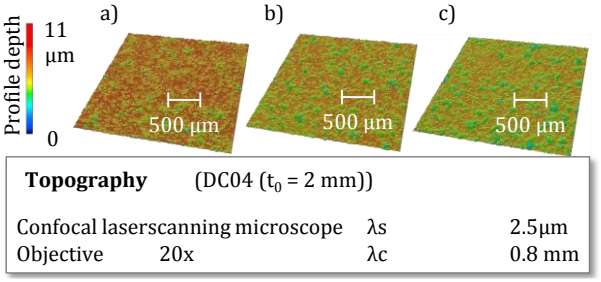

Fig. 9. Topographies after application of 250 N/mm² nominal contact load for a) 0 %, b) 50 % b) 75 % bulk stress.

Fig. ***10*** depicts R_{a_ref} for DP600. It can be observed that for p_{mean} = 100 and 250 N/mm² and all bulk stress values no significant decrease of R_{a_ref} is provided. It should be noted that DP600 has a higher yield strength than DC04. This is clarified by Table 1 and Table 2, which show the Hockett-Sherby parameters for both materials. Consequently, as p_{mean} = 100 and 250 N/mm² are low, no significant flattening of the roughness peaks are observed. For the higher pressure values of 500, 750 and 1000 N/mm² and all investigated bulk stress values a decrease of roughness with increasing load and bulk stress can be observed. Thus, for high contact loads and bulk stresses, the experimental results obtained for DP600 are similar to those obtained for DC04.

Comparing DC04 and DP600, differences are given by the degree of change. The R_{a_ref} values for DC04 are lower than for DP600. Thus, the surface smoothening of DC04 is higher than that of DP600. The R_{a_ref} value for a nominal contact load of 500 N/mm² combined with a bulk stress of $0{\cdot}\sigma_0$ exemplary amounts to 0.44 ± 0.01 for DC04. The R_{a_ref} for DP600 has a value of 0.88 ± 0.03. Thus, the reduction of roughness for DC04 is twice as high than the one for DP600. This can be explained by the different material properties. The initial yield strength of DC04 amounts to 185 N/mm². The value for DP600 is much higher and amounts to 385 N/mm². According to Eq. (16), the hardness is proportional to the yield strength. Thus, smoothing of the surface is strongly influenced by the material properties.

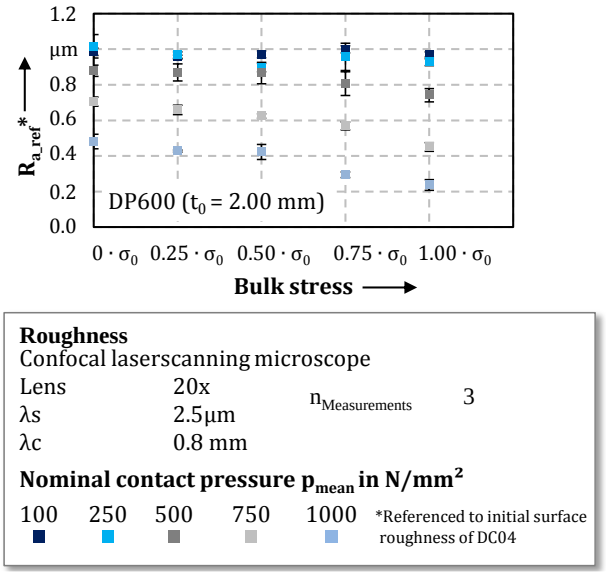

Fig. 10. Average roughness values in dependence on bulk stress and nominal contact load referenced to initial surface roughness for DP600.

All in all it can be stated that the smoothing of the surface is significantly influenced by the applied bulk stress, the nominal contact load and the workpiece material. An application of a nominal contact load on pre-strained workpiece material leads to an increase of the surface smoothing in comparison to the application of just a nominal load. These experimentally determined values validate the results of the numerical investigation in Sec. 4.2.

Table 1. Hockett-Sherby parameters for DC04.

Parameter	Value
σ_0	185 N/mm²
σ_∞	577 N/mm²
a_{HS}	2.1771
b_{HS}	0.6667

Table 2. Hockett-Sherby parameters for DP600.

Parameter	Value
σ_0	385 N/mm^2
σ_∞	1050 N/mm^2
a_{HS}	2.30
b_{HS}	0.6667

4.2 Numerical Results

The surfaces for the contact simulation were measured with a laser microscope Keyence VK-X105. The measured surfaces with $L_x \approx 2.63$ mm and $L_y \approx 2.81$ mm were obtained with $N_x \approx 3700$ and $N_y \approx 3900$ points. In order to perform the simulations in reasonable time, all surfaces were sampled down to $N_x = N_y = 256$ with $L_x = L_y = 2.56$ mm, which is similar to a low pass filtering. The transformation alters the surface roughness of the DC04 blank to $R_a = 1.089$ µm and $R_q = 1.329$ µm, and of the DP600 blank to $R_a = 0.907$ µm and $R_q \approx 1.107$ µm. The parameters of the tool surface are $R_a = 0.126$ µm and $R_q = 0.154$ µm. The tool surface is considered solely elastic, whereas the DC04 surface as well as the DP600 surface are modelled elastic-plastic with the Hockett-Sherby hardening law. Table 1 shows the parameters for DC04, which were identified by Schmaltz with the help of biaxial tests in [28]. Table 2 provides the parameters for DP600, which are based on the flow stress curve given in [29]. The remaining material parameters are $E = 210000$ N/mm^2 and $\nu = 0.30$ for every contact partner. The characteristic length was set to $\lambda = 6 \cdot R_q$. In order to determine λ, R_q is evaluated with the added height field of both tool and workpiece. The bulk stress σ_x is set in dependency on the initial yield stress of the workpiece from 0 to $1.0 \cdot \sigma_0$ in steps of $0.25 \cdot \sigma_0$. The maximum nominal contact load constitutes 750 N/mm^2 and 1000 N/mm^2 for the DC04 surface and the DP600 surface, respectively. The normal load is always applied incrementally in steps of 10 N/mm^2. The parameter β is set to 2.8, because Eq. (22) reduces to Eq. (16) for $\sigma_x = 0$ N/mm^2. Finally, the last parameter γ is equal to 2.3.

The changes of R_a and R_q for DC04 are shown in Fig. 11 to Fig. 20. These figures depict a comparison between the results of the simulations and the experiments.

Both the simulations and the experiments approach $R_a \approx 0.19$ µm and $R_q \approx 0.25$ µm for high contact loads, which is in the magnitude of the tool surface. Furthermore, the surface roughness diminishes with increasing σ_x. The differences between the simulation and the experiments are negligible for $\sigma_x \leq 0.50 \cdot \sigma_0$. For $\sigma_x > 0.50 \cdot \sigma_y$ discrepancies are observable for $p_{mean} = 250$ N/mm^2. Apart from this, the comparison indicates a very high agreement between the experiments and the simulations.

The results of DP600 also highly agree. The comparison is shown in Fig. 21 to Fig. 30. In contrast to the DC04 results, the differences between the simulations and the experiments are negligible in the whole range from $\sigma_x = 0$ to $\sigma_x = \sigma_0$.

All in all, the results indicate the ability of the contact model to successfully determine the surface smoothing in dependency on the nominal normal load and the tensile bulk stress.

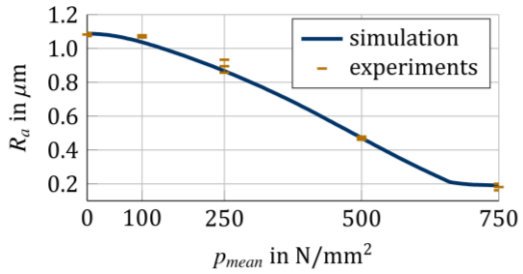

Fig. 11. R_a of DC04-surface with $\sigma_x = 0$.

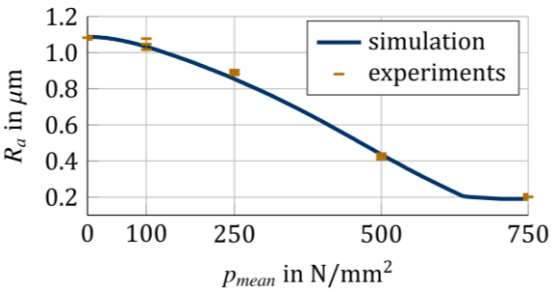

Fig. 12. R_a of DC04-surface with $\sigma_x = 0.25 \cdot \sigma_0$

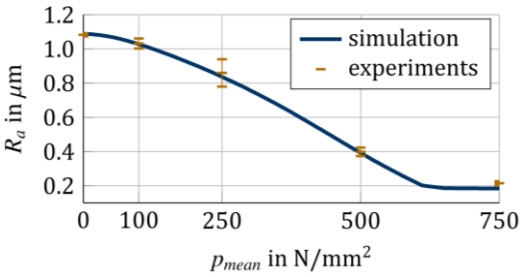

Fig. 13. R_a of DC04-surface with $\sigma_x = 0.50 \cdot \sigma_0$

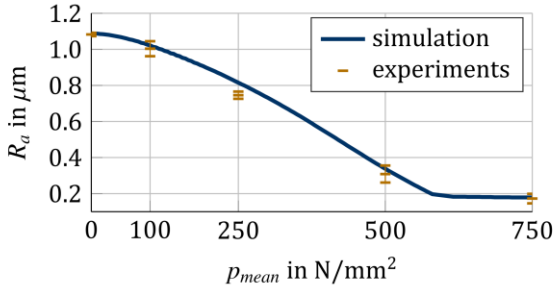

Fig. 14. R_a of DC04-surface with $\sigma_x = 0.75 \cdot \sigma_0$.

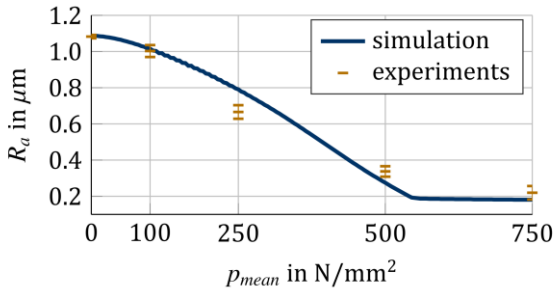

Fig. 15. *R_a of DC04-surface with $\sigma_x = \sigma_0$.*

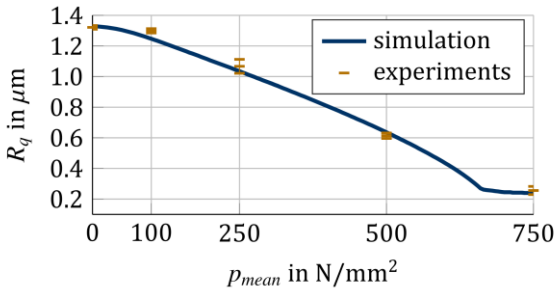

Fig. 16. R_q of DC04-surface with $\sigma_x = 0$.

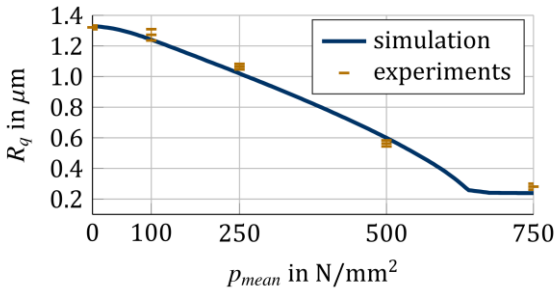

Fig. 17. R_q of DC04-surface with $\sigma_x = 0.25 \cdot \sigma_0$.

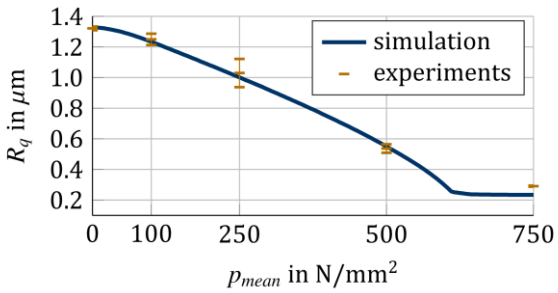

Fig. 18. R_q of DC04-surface with $\sigma_x = 0.50 \cdot \sigma_0$.

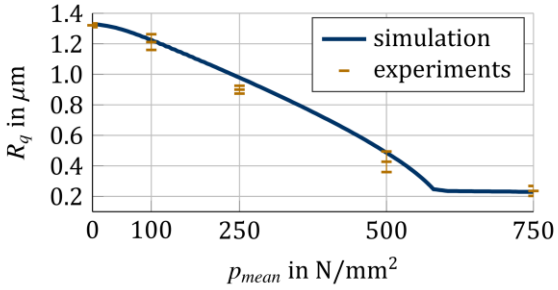

Fig. 19. R_q of DC04-surface with $\sigma_x = 0.75 \cdot \sigma_0$.

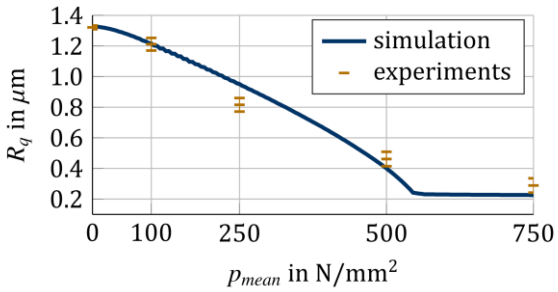

Fig. 20. R_q of DC04-surface with $\sigma_x = \sigma_0$.

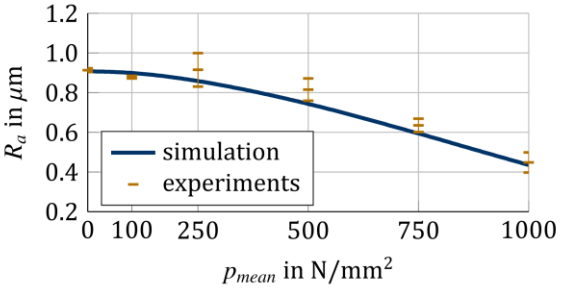

Fig. 21. R_a of DP600-surface with $\sigma_x = 0 \cdot \sigma_0$.

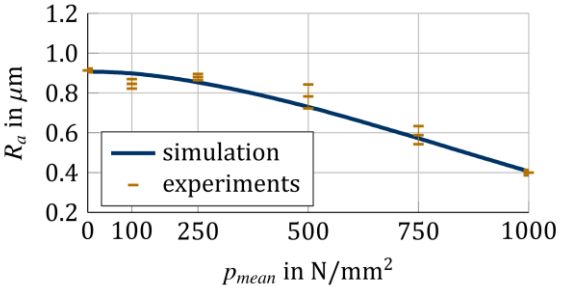

Fig. 22. R_a of DP600-surface with $\sigma_x = 0.25 \cdot \sigma_0$.

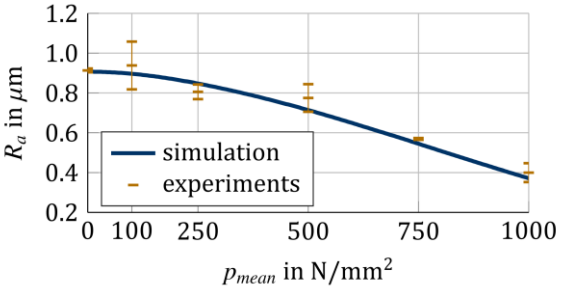

Fig. 23. R_a of DP600-surface with $\sigma_x = 0.50 \cdot \sigma_0$.

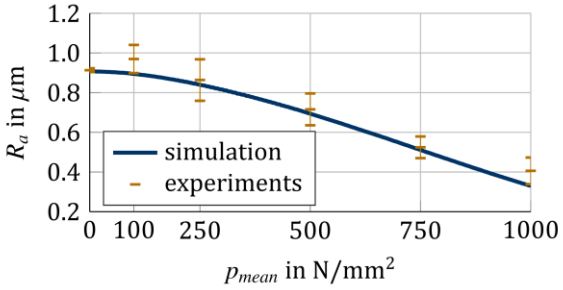

Fig. 24. R_a of DP600surface with $\sigma_x = 0.75 \cdot \sigma_0$.

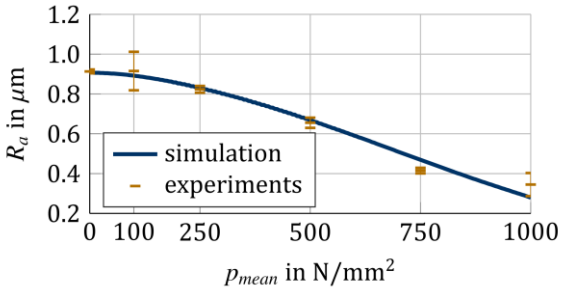

Fig. 25. R_a of DP600-surface with $\sigma_x = \sigma_0$.

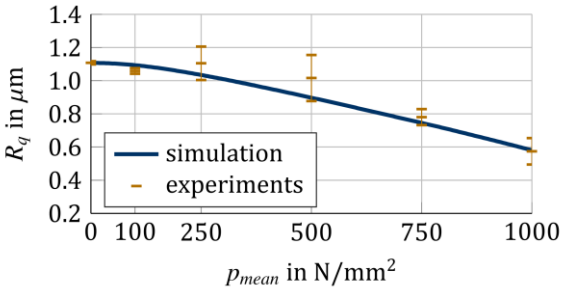

Fig. 26. R_q of DP600-surface with $\sigma_x = 0$.

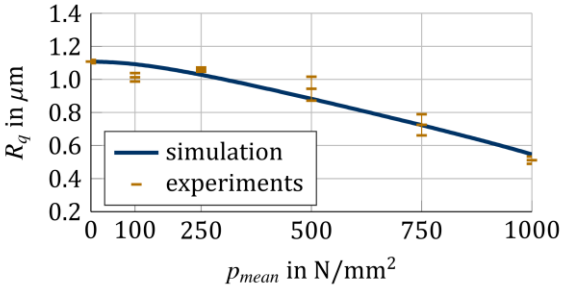

Fig. 27. R_q of DP600-surface with $\sigma_x = 0.25 \cdot \sigma_0$.

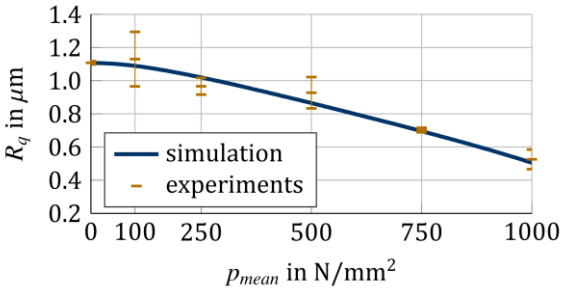

Fig. 28. R_q of DP600-surface with $\sigma_x = 0.50 \cdot \sigma_0$.

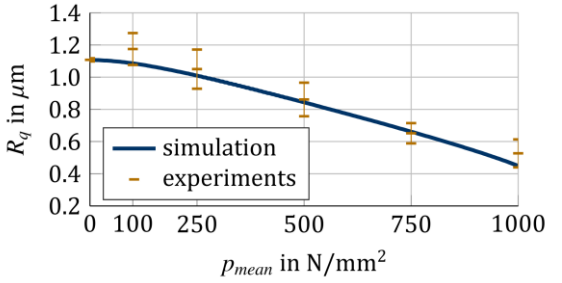

Fig. 29. R_q of DP600-surface with $\sigma_x = 0.75 \cdot \sigma_0$.

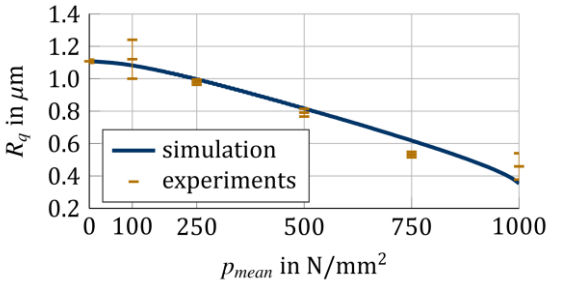

Fig. 30. R_q of DP600-surface with $\sigma_x = \sigma_0$.

4.3 Proposal Of A Modified Friction Law

In this section the CFL is extended based on the results of Sec. 0. The CFL describes the resulting friction shear stress with Eq. (1) in dependency on α. The identification of α is easily derived with the half-space model and simpler than an experimental identification.

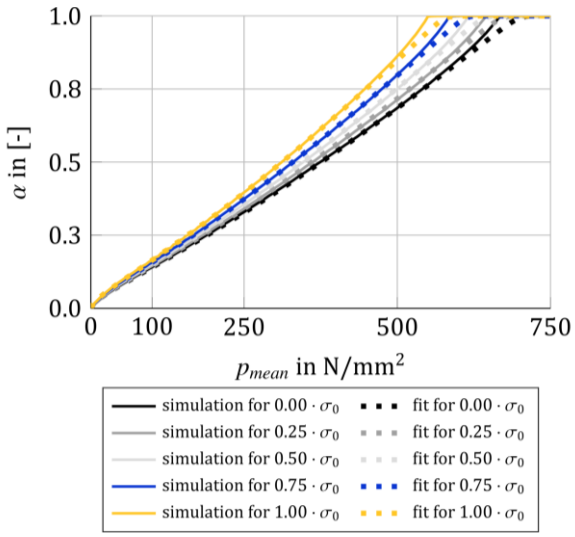

Fig. 31. Fraction of real contact area for DC04.

Fig. **31** shows the contact ratio for DC04 as well as a curve fit which is defined by:

$$\alpha = \sqrt[a_1]{\tanh\left(b_1 \cdot \left(\frac{p_{mean}}{H_0}\right)^{c_1} \cdot \left(\frac{H}{H_0}\right)^{d_1} \cdot \left(1 - \frac{\sigma_x}{H_0}\right)^{e_1}\right)^{a_1}}. \quad (23)$$

Therewith, α is not only a function of the normalized normal load p_{mean}/H_0, but also a function of the normalized current hardness H/H_0 and the normalized bulk stress σ_x/H_0. The parameters a_1, b_1, c_1, d_1 and e_1 are identified with the least squares method and shown in Table 3.

Table 3. Coefficients for α for initial contact.

Material	Coefficient				
	a_1	b_1	c_1	d_1	e_1
DC04	20	0.382	0.684	2.295	-0.264
DP600	20	0.386	0.617	3.0976	-0.216

The contact ratio for DP600 and the corresponding curve fit are shown in Fig. 32.

As already mentioned, the friction model is able to consider un-/reloading. In order to retain this explicit feature, Eq. (3) is analogously to Eq. (2) enhanced to:

$$\alpha = \sqrt[a_2]{\tanh\left(\frac{b_2}{\alpha(p_h, H_h, \sigma_{x,h})} \cdot \left(\frac{p_{mean}}{H_0}\right)^{c_2} \cdot \left(\frac{H}{H_0}\right)^{d_2}\right)^{a_2}} \cdot \alpha(p_h, H_h, \sigma_{x,h}), \quad (24)$$

where $\alpha(p_h,H_h,\sigma_{x,h})$ is the share between the real contact area and the apparent area. The latter occurs at the maximum contact pressure p_h of former contacts. The hardness H_h and the bulk stress $\sigma_{x,h}$ also describe the condition when the maximum contact pressure takes place. The parameters in Eq. (24) are also evaluated numerically and shown in Table 4. It must be noted that Eq. (24) does not depend on the normalized bulk stress, since the coefficient of $\sigma_x/H_0 \approx 0$ for both DC04 and DP600. A choice of four examples showing the conformity of Eq. (24) is presented in Fig. 33 to Fig. 36. Fig. 33 and Fig. 34 show α for DC04 with $\sigma_x = 0$ and $0.50\cdot\sigma_0$, respectively. Besides initial contact, un-/reloading with p_h ranging from 100 N/mm² to 500 N/mm² in steps of 100 N/mm² is depicted. Fig. 35 and Fig. 36 show α for DP600 with $\sigma_x = 0.25\cdot\sigma_0$ and $0.75\cdot\sigma_0$, respectively. The maximum historic pressure ranges for DP600 from 100 N/mm² to 700 N/mm² in steps of 100 N/mm².

Table 4. Coefficients for α for un- & reloading.

Material	Coefficient			
	a_2	b_2	c_2	d_2
DC04	3.069	0.618	0.765	1.811
DP600	2.368	0.710	0.722	1.688

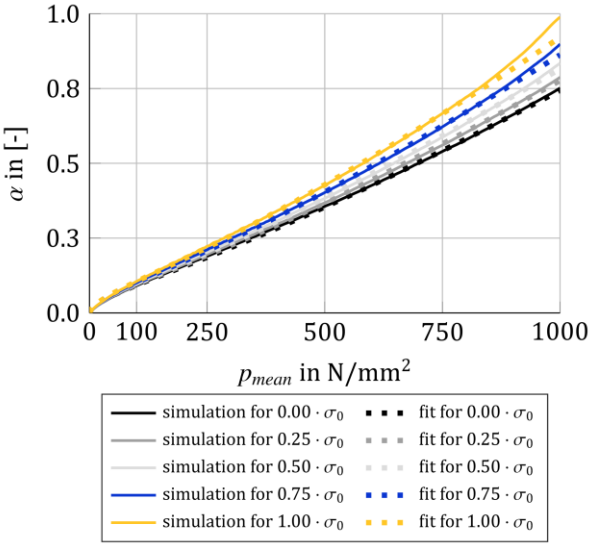

Fig. 32. Fraction of real contact area for DP600.

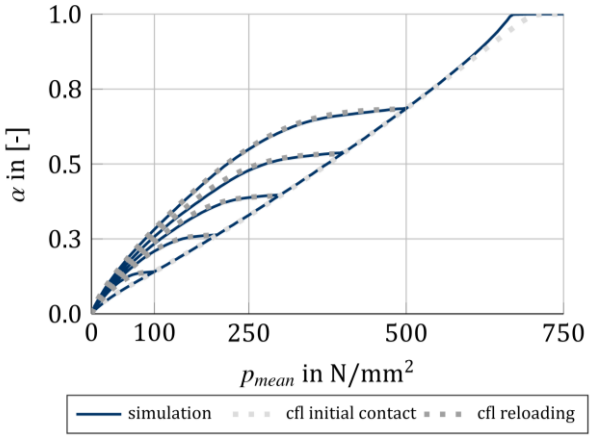

Fig. 33. α for DC04 and $\sigma_x = 0\cdot\sigma_y$.

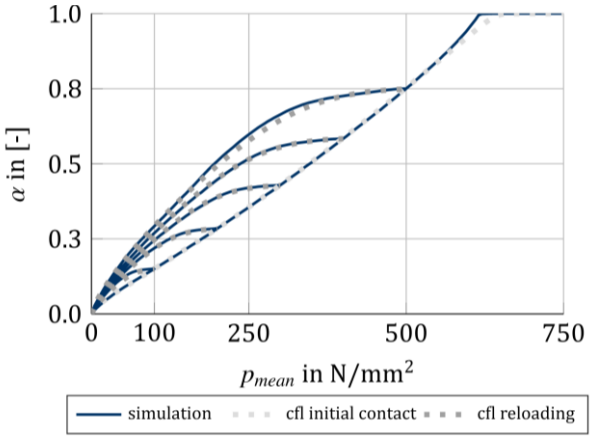

Fig. 34. α for DC04 and $\sigma_x = 0.50\cdot\sigma_y$.

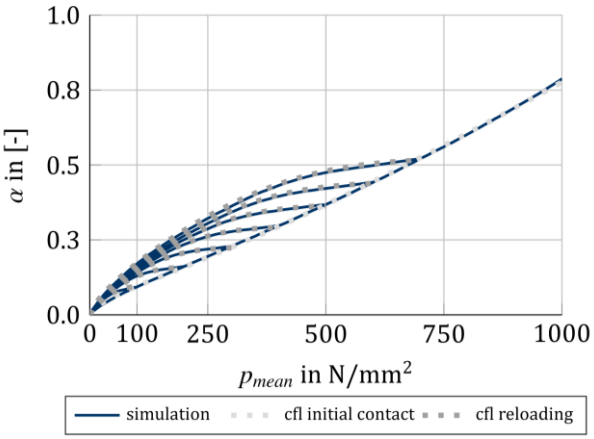

Fig. 35. α for DP600 and $\sigma_x = 0.25 \cdot \sigma_y$.

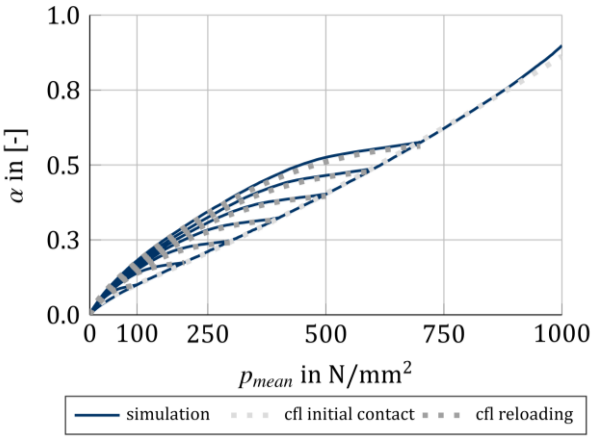

Fig. 36 α for DP600 and $\sigma_x = 0.75 \cdot \sigma_y$.

5. CONCLUSION

The experimental study of this work investigates the influence of bulk stresses on the plastic surface smoothing of electric discharge textured sheet metal. The experimental setup is able to apply a tensile stress, which ranges between 0 and flow stress, to the blank. Simultaneously, the surface of the sheet metal is brought into contact with a stamp which is much harder than the sheet sample. The plastic smoothing of the sheet metal that is characterized by R_a and R_q indicates a dependency on the normal load and on the bulk stress. A half-space model which is enhanced to take into account work hardening is used to model the experimental outcome. The half-space model is able to successfully simulate the change of the surface roughness for both DC04 and DP600 with minor deviations. The half-space model can also identify the ratio between the real contact area and the apparent area. The ratio is a function of the normalized normal load, the normalized current hardness, and the normalized bulk stress. This fit can be combined with the CFL, as the CFL is the product of the shear strength and the contact ratio. This approach fulfils the demand to evaluate the resulting friction shear stress in dependency on the bulk stress.

Acknowledgement

We gratefully thank the German Research Foundation (DFG) for their support of project C1 of the transregional collaborative research centre (Transregio) 73 that researches the topic of sheet-bulk-metal-forming.

REFERENCES

[1] A. Westeneng, 'Modelling of Contact and Friction in Deep Drawing Processes', *PhD thesis*, University of Twente, Enschede, 2001.

[2] J. Hol, 'Multi-scale friction modelling for sheet metal forming', *PhD thesis*, University of Twente, Enschede, 2013.

[3] E. Vidal-Sallé, L. Baillet and J.C. Boyer, 'Friction law for hydrostatic mixed lubrication regime', *Journal of Materials Processing Technology*, vol. 118, no. 1-3, pp. 101-108, 2001.

[4] M. Merklein, J. Allwood, B.-A. Behrens, A. Brosius, H. Hagenah, K. Kuzman, K. Mori, A.E. Tekkaya and A. Weckenmann, 'Bulk forming of sheet metal', *CIRP Annals – Manufacturing Technology*, vol. 61, no. 2, pp. 725-745, 2012.

[5] M.C. Shaw, 'The role of friction in deformation processing', *Wear*, vol. 6, no. 2, pp. 140-158, 1963.

[6] M.C. Shaw, A. Ber and P.A. Mamin, 'Friction Characteristics of Sliding Surfaces Undergoing Subsurface Plastic Flow', *Journal of Basic Engineering*, vol. 82, no. 2, 342-345, 1960.

[7] T. Wanheim, N. Bay and S.A. Petersen, 'A theoretically determined model for friction in metal working processes', *Wear*, vol. 28, no. 2, pp. 251-258, 1974.

[8] T. Wanheim and N. Bay, 'A Model for Friction in Metal Forming Prcoesses', *CIRP Annals – Manufacturing Technology*, vol. 27, pp. 189-194, 1978.

[9] F. Beyer, F. Hauer and K. Willner, 'Development of a Constitutive Friction Law based on the Frictional Interaction of Rough Surfaces', *Tribology in Industry*, vol. 37, no. 4, pp. 400-412, 2015.

[10] M. Vilotić, D. Kakaš, P. Terek, L. Kovačević, and A. Miletić, 'Neutral Radius Value Determination by Numerical Simulation Method at Ring Upsetting Test', *Tribology in Industry*, vol. 33, no. 3, pp. 122-127, 2011.

[11] L. Pei, S. Hyun, J.F. Molinari and M.O. Robbins, 'Finite element modelling of elasto-plastic contact between rough surfaces', *Journal of the Mechanics and Physics of Solids*, vol. 53, no. 11, pp. 2385-2409, 2005.

[12] B. Chatterjee and P. Sahoo, 'Elastic-plastic Contact of a Deformable Sphere Against a Rigid Flat for Varying Material Properties Under Full Stick Contact Condition', *Tribology in Industry*, vol. 33, no. 4, pp. 164-172, 2011.

[13] B. Chatterjee and P. Sahoo, 'Shakedown Behavior in Multiple Normal Loading-Unloading of an Elastic-Plastic Spherical Stick Contact', *Tribology in Industry*, vol. 35, no. 1, pp. 3-18, 2013.

[14] J.J. Kalker, 'Three-Dimensional Elastic Bodies in Rolling Contact', Springer Netherlands, Dordrecht, 1990.

[15] X. Tian and B. Bhushan, 'A Numerical Three-Dimensional Model for the Contact of Rough Surfaces by Variational Principle', *Journal of Tribology*, vol. 118, no. 1, pp. 33-42, 1996.

[16] J. Boussinesq, 'Applications des potentiels à l'étude de l'équilibre et du mouvement des solides èlastiques', Gauthier-Villars, 1885.

[17] A.E.H. Love, 'The Stress produced in a Semi-infinite Solid by Pressure on Part of the Boundary', *Philosophical Transactions of the Royal Society of London. Series A, Containing Papers of a Mathematical of Physical Character*, vol. 228, pp. 377-420, 1929.

[18] J.M. Allwood, 'Survey and Performance Assessment of Solution Methods for Elastic Rough Contact Problems', *Journal of Tribology*, vol. 127, no. 1, pp. 10-23, 2005.

[19] F.P. Bowden and D. Tabor, 'The friction and lubrication of solids', Clarendon Press and Oxford University Press, Oxford and New York, 1954.

[20] F. Hauer, 'Die elasto-plastische Einglättung rauer Oberflächen und ihr Einfluss auf die Reibung in der Umformtechnik', *PhD thesis*, Chair of Applied Mechanics, Friedrich-Alexander-Universität Erlangen-Nürnberg, Erlangen, 2014.

[21] J.E. Hockett and O.D. Sherby, 'Large strain deformation of polycrystalline metals at low homologous temperatures', *Journal of the Mechanics and Physics of Solids*, vol. 23, no. 2, pp. 87-98, 1975.

[22] J. Pullen and J.B. Williamson, 'On the Plastic Contact of Rough Surfaces', *Proceedings of the Royal Society A: Mathematical, Physical and Engineering Sciences*, vol. 327, no. 1569, pp. 159-173, 1972.

[23] C. Jacq, D. Nelias, G. Lormand and D. Girodin, 'Development of a Three-Dimensional Semi-Analytical Elastic-Plastic Contact Code', *Journal of Tribology*, vol. 124, no. 4, pp. 653-667, 2002.

[24] D. Nèlias, V. Boucly and M. Brunet, 'Elastic-Plastic Contact Between Rough Surfaces: Proposal for a Wear or Running-in Model', *Journal of Tribology*, vol. 128, no. 2, p. 236-244, 2006.

[25] K.L. Johnson, 'Contact Mechanics', Cambridge University Press, Cambridge, 1985.

[26] F. Wang and L.M. Keer, 'Numerical Simulation for Three-dimensional Elastic-Plastic Contact with Hardening Behavior', *Journal of Tribology*, vol. 127, no. 3, pp. 494-502, 2005.

[27] D. Tabor, 'Junction Growth in Metallic Friction: The Role of Combined Stresses and Surface Contamination', *Proceedings of the Royal Society A: Mathematical, Physical and Engineering Sciences*, vol. 251, no. 1266, pp. 378-393, 1959.

[28] S. Schmaltz and K. Willner, 'Comparison of Different Biaxial Tests for the Inverse Identification of Sheet Steel Material Parameters', *Strain*, vol. 50, no. 5, pp. 389-403, 2014.

[29] D. Gröbel, P. Hildenbrand, U. Engel and M. Merklein, 'Influence of tailored blanks on forming of cold forged functional elements in a sheet-bulk metal forming process', METEC & 2nd ESTAD 2015, Düsseldorf, Germany, 2015.